Materials Science and Engineering B 311 (2025) 117817

Contents lists available at ScienceDirect

Materials Science & Engineering B

journal homepage: www.elsevier.com/locate/mseb

Unveiling the impact of Se based HTM on $BaZrSe_3$ perovskites solar cell and improving the theoretical efficiency above 32%

Md Masum Mia [a], Md. Faruk Hossain [b], Mahabur Rahman [a], Nacer Badi [c], Ahmad Irfan [d], Md. Ferdous Rahman [a,*]

[a] Advanced Energy Materials and Solar Cell Research Laboratory, Department of Electrical and Electronic Engineering, Begum Rokeya University, Rangpur 5400, Bangladesh
[b] Department of Physics, Rajshahi University of Engineering & Technology, Rajshahi 6204, Bangladesh
[c] Thermal Management and Sustainability Research Laboratory, Department of Physics, Faculty of Science, University of Tabuk, Tabuk 71491, Saudi Arabia
[d] Department of Chemistry, College of Science, King Khalid University, Abha 61413, P.O. Box 9004, Saudi Arabia

ARTICLE INFO

Keywords:
Chalcogenide
$BaZrSe_3$
SCAPS-1D
Hole transport material
Quantum efficiency
Solar cell

ABSTRACT

In light of growing global energy demands and the environmental challenges posed by fossil fuels, this study investigates the efficiency improvement of $BaZrSe_3$-based perovskite solar cells (PSCs) through the application of selenium (Se)-based hole transport materials (HTMs). Chalcogenide perovskites, such as $BaZrSe_3$, present a viable alternative to conventional photovoltaic materials that are often toxic and scarce. Using SCAPS-1D simulations, we modeled and analyzed the photovoltaic performance of PSCs incorporating different Se-based HTMs, including GeSe, $MoSe_2$, Sb_2Se_3, and SnSe. The results show that integrating SnSe as the HTM significantly enhances power conversion efficiency (PCE), reaching a theoretical maximum of 32.20%. In contrast, $BaZrSe_3$-based PSCs without HTMs (FTO/CdS/$BaZrSe_3$/Au) achieved a PCE of 23.63%. The performance boost is attributed to better band alignment, improved carrier transport, and reduced recombination losses enabled by the SnSe layer. This study underscores the potential of Se-based HTMs in advancing $BaZrSe_3$-based PSCs, paving the way for sustainable and highly efficient photovoltaic technologies.

1. Introduction

As the population grows, the demand for energy has significantly increased, primarily dependent on fossil fuels [1]. This finite energy source has caused several problems, including pollution, health issues and global warming. However, solar energy, being a clean energy source that is completely renewable and inexhaustible with no associated costs, is crucial for fulfilling the future energy demands [2–5]. Recent research advancements have therefore driven an increased reliance on solar energy, enhancing its efficiency and stability. Moreover, the potential of photo-assisted rechargeable metal batteries is also explored, with a focus on their limitations and future possibilities, underscoring their promise as an innovative and inexpensive solution for energy conversion and storage [6–9]. CdTe and CIGS (copper indium gallium selenide) solar cells are currently dominating the thin-film technology market [10–12]. However, cadmium and tellurium are toxic, and indium and gallium are scarce. Therefore, non-toxic and abundant alternatives like CZTS (copper zinc tin sulfide) is a promising solar energy material owing to its simple synthesis with the non-toxic and stable kesterite structure [13]. Moreover, it possesses favorable optoelectronic characteristics, including an adjustable bandgap, high hole mobility and the use of elements readily available on Earth [14,15]. Despite these advantages, CZTS-based solar cells suffer from a shortfall in achieving greater conversion efficiency due to a low open-circuit voltage (V_{oc}) [16]. Organic-inorganic mixed perovskite solar cells (PSCs) have rapidly achieved a significant power conversion efficiency (*PCE*) of 25.8 %, surpassing many other semiconductors solar cell [17–19]. However, their commercialization is hindered by the existence of poisonous lead (Pb) and instability matters caused by heat, moisture and electric fields, prompting the search for alternate materials for photovoltaic devices.

Recently, chalcogenide perovskites with the formula AMX_3 (where 'X' can be either S or Se and 'A' and 'M' represent two cations of different sizes) have emerged as an innovative material for PSC applications owing to their extremely resilient properties [20] together with outstanding charge transport characteristics, robust optoelectronic properties and effectively produced via experimental techniques [21].

* Corresponding author.
E-mail address: ferdousapee@gmail.com (Md. Ferdous Rahman).

https://doi.org/10.1016/j.mseb.2024.117817
Received 16 August 2024; Received in revised form 3 November 2024; Accepted 6 November 2024
Available online 13 November 2024

These materials are regarded as more eco-friendly compared to lead halide perovskites [22]. Among the emerging candidates, $BaZrSe_3$-based chalcogenide perovskites have demonstrated promising features, including suitable band gaps, high absorption coefficients and intrinsic stability [23,24]. Korbel et al. [25] reported that the bandgap of $BaZrSe_3$ is 1.01 eV, allowing the material to absorb a significant portion of the solar spectrum, especially in the near-infrared region, where a large fraction of the sun's energy is concentrated. Despite these advantages, the efficiency of $BaZrSe_3$-based PSCs still lags behind their theoretical potential, necessitating innovative approaches to device architecture optimization.

One such approach is the implementation of selenium (Se)-based hole transport materials (HTMs) layers. Using an HTM which also functions as a back surface field (BSF) layer is an effective strategy to enhance cell output while reducing manufacturing expenses. HTM layers are crucial in solar cell design as they enhance carrier collection, reduce recombination losses and improve open-circuit voltage (V_{oc}) [26,27]. Se-based materials, with their excellent electrical properties and ability to form effective heterojunctions, present a compelling option for HTM layers in chalcogenide PSCs. The integration of Se-based HTM is expected to improve carrier dynamics, thereby reducing recombination and facilitating higher carrier extraction efficiency because they have efficient electron-hole generation and separation characteristics [28]. Cadmium sulfide (CdS) is used as the electron transport material (ETM) in this research instead of titanium dioxide (TiO_2) because CdS offers higher electron mobility compared to TiO_2 [29]. A higher mobility ETM is essential for improving charge extraction, reducing recombination losses, enhancing fill factor, increasing stability, and optimizing the overall efficiency of perovskite solar cells.

This study focuses on understanding the impact of Se-based HTM layers on the performance of $BaZrSe_3$-based PSCs and exploring strategies to push the efficiency beyond 32 %. In order to do that, we employ a rigorous simulation methodology using SCAPS-1D to model and analyze the output parameters of the planned device architecture of Glass/FTO/CdS/$BaZrSe_3$/Au and Glass/FTO/CdS/$BaZrSe_3$/HTM/Au, where the HTM layer is composed of different materials such as GeSe, $MoSe_2$, Sb_2Se_3, and SnSe. This simulation-based investigation aims to identify the optimal HTM by systematically varying and analyzing the mentioned configurations to maximize device efficiency paving the method for high-performance, lead-free chalcogenide PSCs.

2. Methodology

2.1. Numerical simulations

For our research, we utilized SCAPS-1D version of 3.3.07, a simplistic solar cell simulation tool renowned for its capability to model the electronic and optical characteristics of PSCs providing detailed insights into the mechanisms that govern their performance engineered by Professor Marc Burgelman [30]. The fundamental physics behind SCAPS involves solving one-dimensional equations for semiconductor such as Poisson's, and continuity equation, while accounting for one or more recombination mechanisms are shown from Eqs. (1) to (3)[31,32] In this whole study, the AM 1.5 illumination spectrum was employed to simulate realistic sunlight conditions, while the operational temperature was carefully controlled and consistently maintained at 300 K to ensure accurate and reliable measurement of the photovoltaic performance.

Poisson equation:

$$\frac{d^2\varphi}{dx^2} = \frac{\rho(x)}{\varepsilon_s} = -\frac{q}{\varepsilon_s}(p - n + ND - NA) \tag{1}$$

Continuity equation for electrons:

$$J_n = q\mu_n n\frac{\partial\varphi}{\partial x} + qD_n\frac{\partial n}{\partial x} \tag{2}$$

Continuity equation for holes:

$$J_p = q\mu_p p\frac{\partial\varphi}{\partial x} - qD_p\frac{\partial p}{\partial x} \tag{3}$$

Where, φ = electrical potential, ρ = charge density, ε_s = the permittivity of the semiconductor, N_A = acceptor, N_D = donor density, n = electron concentrations, p = hole concentrations, J_p = hole current density, J_n = electron current density, $D_{p,n}$ = hole and electron diffusion coefficient, q = electric charge, $\mu_{p,n}$ = hole and electron mobility [33].

2.2. Device Arrangement

The configuration of the solar cell is a valuable matter in assessing the performance of chalcogenide PSCs. The configuration of PSC under this study comprises a fluorine-doped tin oxide (FTO)/buffer, (CdS)/absorber, (perovskite)/hole transport material (HTM). The cell's schematic structure is depicted in Fig. 1(a-b) without HTM and with HTM. In this design, the perovskite material is positioned between an electron transport material (ETM), which is CdS, and HTM. The CdS layer extracts negative charge carriers (electrons), while the HTM extracts positive charge carriers (holes). The thickness of FTO is chosen as 50 nm as it is optimized in the previous literature [34]. Au (Gold) is also applied as a rear contact which has work function of 5.1 eV in our solar cells to ensure the efficient collection and transportation of the generated charge carries. Table 1 displays the different significant parameters of various materials employed in this simulation, encompassing electron and hole mobilities, electron affinities, relative permittivity, effective density of states (DOS), acceptor and donor densities, as well as crystalline phase. The detailed of interfaces parameters for both configuration of $BaZrSe_3$-based PSCs are in Table 2.

3. Results and Discussion

The simulation was conducted to compare various cell structures by altering the BSF/HTM materials to identify the most efficient and stable CdS/$BaZrSe_3$ solar cell configuration. We evaluated four cell structures by incorporating semiconductor materials such as GeSe, $MoSe_2$, Sb_2Se_3 and SnSe as HTM layers, to assess their performance. This section examines the effect of several factors on the device's output parameters.

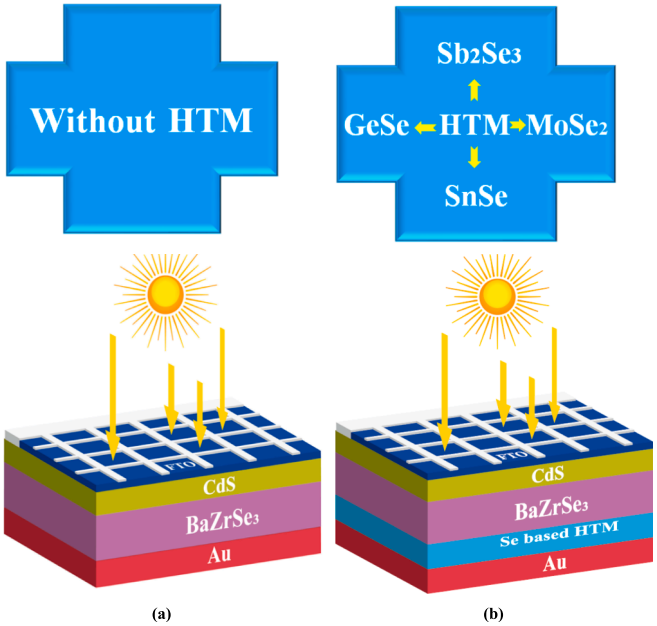

Fig. 1. Device architecture of $BaZrSe_3$-based PSCs (a) without HTM and (b) with HTM.

Table 1
Simulation parameters of the solar cell [35,36,37,38,39,20].

Parameters (units)	FTO	CdS	$BaZrSe_3$	SnSe	Sb_2Se_3	$MoSe_2$	GeSe
Thickness (nm)	50	50	1000	100	100	100	100
Bandgap (eV)	3.6	2.4	1.01	1.2	1.2	1.10	1.14
Electron affinity (eV)	4	4.2	4.5	4.2	4.16	4.14	4.07
Dielectric permittivity	9	10	4.19	12.50	14.50	13.6	15.3
CB effective DOS (cm^{-3})	2.2×10^{18}	2.8×10^{19}	2.2×10^{18}	1.75×10^{18}	2.0×10^{18}	2.2×10^{18}	4.0×10^{18}
VB effective DOS (cm^{-3})	1.8×10^{19}	2.8×10^{19}	1.8×10^{19}	4.57×10^{18}	1.0×10^{19}	1.8×10^{19}	1.75×10^{19}
Electron mobility ($cm^2V^{-1}s^{-1}$)	100	100	11.3	130	16.7	100	12.7
Hole mobility ($cm^2V^{-1}s^{-1}$)	25	25	5.8	56.7	16.7	25	11.2
Donor density, N_D (cm^{-3})	5×10^{18}	1×10^{18}	0	0	0	0	0
Acceptor density, N_A (cm^{-3})	0	0	1×10^{16}	1×10^{16}	1×10^{13}	1×10^{16}	1×10^{16}
Defect type	acceptor	acceptor	donor	donor	donor	donor	donor
Bulk defect density, Nt (cm^{-3})	10^{14}	10^{18}	10^{12}	10^{10}	10^{10}	10^{10}	10^{10}
Crystalline phase	tetragonal rutile	hexagonal wurtzite	orthorhombic	orthorhombic	orthorhombic	hexagonal	orthorhombic

Table 2
Interface defect densities parameters applied in the HTM/Absorber & Absorber/ETM Interface.

Parameters (unit)	HTM/Absorber Interface	Absorber/ETM Interface
Defect type	Neutral	Neutral
Electron capture cross- section, σ_e (cm^2)	10^{-19}	10^{-19}
Hole capture cross-section, σ_p (cm^2)	10^{-19}	10^{-19}
Defect position above the highest EV (eV)	0.6	0.6
Defect density (cm^{-2})	10^{10}	10^{10}

These factors include absorber layer thickness, doping density, defect density, thickness of ETM and HTM (in supplementary materials), interface defect density, series and shunt resistance, and temperature.

3.1. Band alignment of $BaZrSe_3$-based heterostructure with various HTMs

Fig. 2(a–f) illustrate the crystal structure and band configuration of various $BaZrSe_3$-based heterostructures, including the quasi-Fermi levels for electrons (F_n) and holes (F_p), as well as the valence band maximum (E_v) and conduction band minimum (E_c). In each ETM type, F_p aligns with E_v, while F_n and E_c maintain a harmonic progression [2,14,40,41] implies that the energy levels are well-aligned throughout the structure, contributing to overall improved performance of the solar cell. Without any HTM, the energy levels show a clear distinction between the conduction and valence bands. The absence of HTM leads to a higher recombination rate due to inefficient hole extraction which reduces the V_{oc}[42]. The introduction of HTM layer modifies the band structure by creating a step-like alignment at the interface. The quasi-Fermi levels (F_n and F_p) suggest efficient isolation and transfer of charge carriers. The band alignment promotes effective hole extraction while maintaining a high open-circuit voltage (V_{oc}) [43,44]. Among the various HTMs explored for this $BaZrSe_3$-based PSCs, SnSe has exhibited most favorable band alignment with minimal energy offset between the perovskite layer and SnSe which facilitates smoother charge transfer [45]. This optimal offset is crucial for reducing energy losses during carrier transport resulting in the maximum *PCE* of 32.20 % attributed to its enhanced absorption, [46] better crystallinity [47] and reduced defect states [48]. Table 3 displayed the obtained photovoltaic parameters quantitively, where $BaZrSe_3$-based PSC with SnSe shows the highest performance which enables us to select SnSe as optimized HTM among the investigated HTMs in our study.

3.2. Impact of Active layer thickness on PSC's output

Given that the performance of PSC is heavily impacted by absorber layer thickness, therefore, it should have an optimal thickness to optimize the photons absorption and electron-hole pairs creation [49]. Fig. 3 demonstrates the photovoltaic output such as *FF*, J_{sc}, V_{oc} vand *PCE* with the variation of absorber thickness, ranging from 0.5 μm to 1.5 μm without HTM and with SnSe HTM applying the other optimized parameters as stated in Table 1.

It is noticed from Fig. 3 (a) that as thickness of the absorber rises, all photovoltaic outputs such as V_{oc}, J_{sc}, *FF*, and *PCE* are enhanced. This means that without HTM, increasing absorber thickness enhances the device performance due to better absorption and lower recombination losses. Conversely, Fig. 3(b) shows that J_{sc} alone rises with the increase in thickness. Without HTMs, at a thickness of 1 μm, the device attains a V_{oc} of 0.62 V, a J_{sc} of 45.96 mA/cm^2, an *FF* of 82.94 %, and a *PCE* of 23.63 %. However, with the HTM SnSe, at the same thickness, the V_{oc} improves to 0.88 V, the J_{sc} to 46.14 mA/cm^2, the *FF* to 79.30 %, and the *PCE* to 32.20 % as indicated in Fig. 3(b). Further increasing the absorber layer thickness reduces the *PCE* influenced by V_{oc} and *FF*. This decrement of V_{oc} is directly affected by carrier recombination and the consistent reduction in *FF* with a thicker absorber layer is attributed to a rise in series resistance [50].

3.3. Impact of acceptor concentration in the absorber

To assess the impact of the acceptor concentration (N_A) in the $BaZrSe_3$ absorber on the performance of PSCs, the N_A was varied from 10^{10} cm^{-3} to 10^{20} cm^{-3}. The results are depicted in Fig. 4(a) and 4(b), showing the device behavior without a hole transport material (HTM) and with SnSe as the HTM, respectively. In Fig. 4(b), with SnSe HTM, the performance metrics remain mostly stable when N_A is less than or equal to10^{10} cm^{-3}. Beyond this concentration, there is an improvement in all parameters up to a threshold, after which they start to decline-except for the open-circuit voltage (Voc), which continues to increase with rising N_A. In contrast, Fig. 4(a), which represents the case without HTM, shows that all photovoltaic parameters remain largely unchanged when N_A is below 10^{16} cm^{-3}. However, above this threshold, all parameters decrease except for Voc. For both scenarios, the observed increase in Voc and decrease in short-circuit current density (Jsc) can be attributed to enhanced recombination at higher absorber carrier concentrations, which reduces the accumulation of photogenerated carriers [23]. In Fig. 4(a), at the optimized N_A of 10^{16} cm^{-3}, the solar cell achieves a (Voc) of 0.62 V, a (Jsc) of 45.96 mA/cm^2, a fill factor (FF) of 82.94 %, and a power conversion efficiency (PCE) of 23.63 %. However, when the SnSe HTM is introduced, as shown in Fig. 4(b), the same N_A of 10^{16} cm^{-3} results in an improved (Voc) of 0.88 V, a (Jsc) of 46.14 mA/cm^2, a FF of 79.30 %, and a PCE of 32.20 %.

The observed shift in the concavity of the FF and PCE curves as a function of carrier concentration is notable. This non-linear behavior has been previously reported in various experimental and theoretical studies on solar cells, where the FF and PCE dependence on carrier concentration is influenced by multiple factors. These factors include recombination dynamics, charge carrier mobility, series resistance, and the

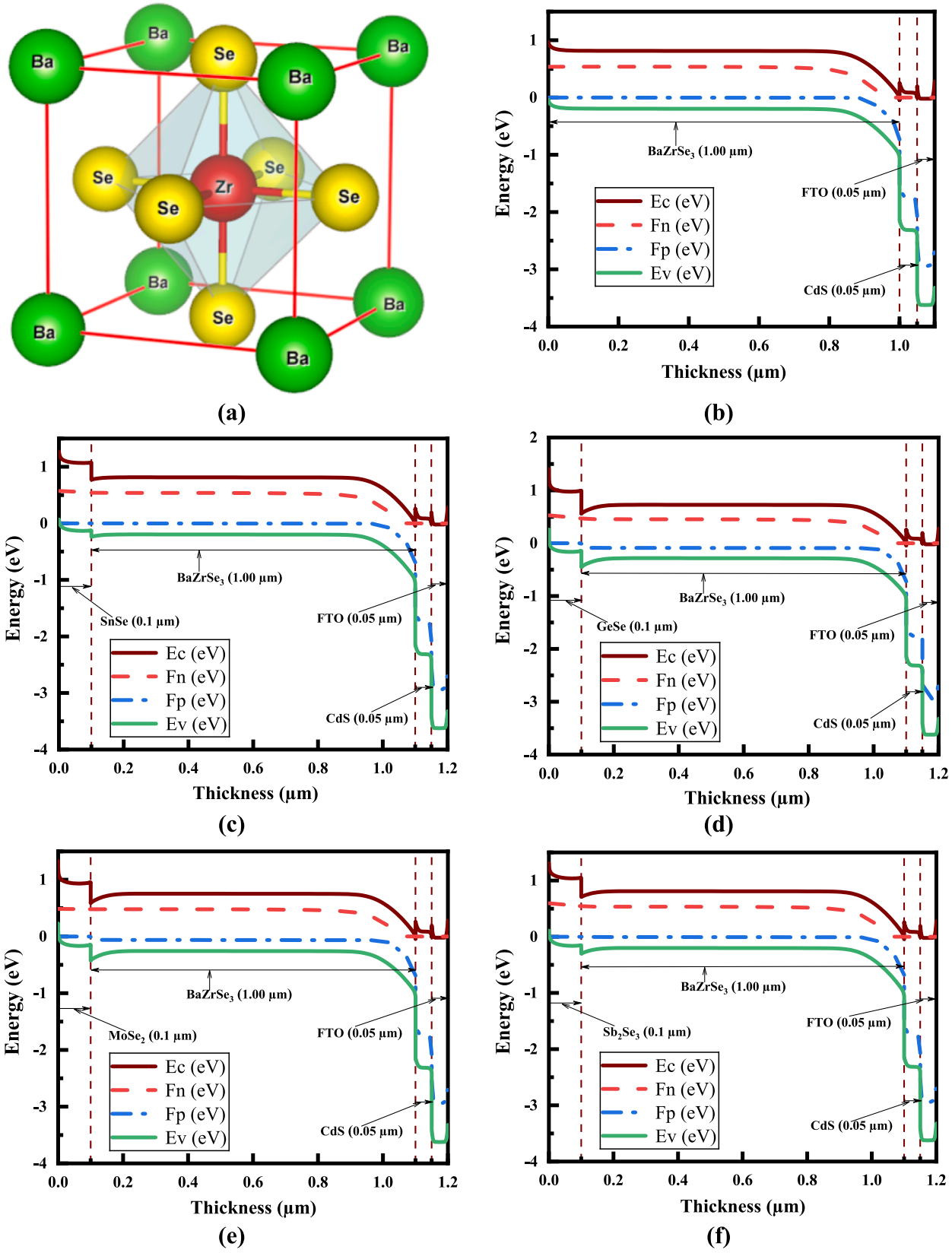

Fig. 2. (a) Crystal structure of $BaZrSe_3$ and, band structure of optimized devices of $BaZrSe_3$ based PSCs (b) without HTM, with HTMs of (c) SnSe, (d) GeSe, (e) $MoSe_2$ and (f) Sb_2Se_3.

Table 3
PV parameters of $BaZrSe_3$-based PSCs for different HTM layer.

HTM Layer	V_{OC} (V)	J_{SC} (mA/cm^{-2})	*FF* (%)	*PCE* (%)
Without HTM	0.62	45.96	82.94	23.63
GeSe	0.82	46.13	77.51	29.32
$MoSe_2$	0.84	46.14	77.85	30.17
Sb_2Se_3	0.88	46.13	78.74	31.96
SnSe	0.88	46.14	79.30	32.20

effect of doping concentration on quasi-Fermi level splitting. Such phenomena are common across different types of solar cells and highlight the complex interplay between doping levels and device performance metrics [51].

3.4. Effect of the defect density of the Active layer

Understanding the effect of defect density (N_t) is crucial because the change of N_t in the absorber meaningfully affects the output of PSC. Fig. 5 illustrates the effect of the defect density in the $BaZrSe_3$ absorber on the simulated solar cell performance metrics, with densities ranging from 10^{10} cm^{-3} to 10^{17} cm^{-3}. In Fig. 5(a), the outcomes show two main trends: (i) performance parameters remain relatively stable when defect density is between 10^{10} cm^{-3} to 10^{13} cm$^{-3,}$ and (ii) a sharp decline in performance occurs from 10^{13} cm^{-3} to 10^{17} cm^{-3}. However, with the HTM in Fig. 5(b), *PCE* declines consistently from defect densities of 10^{10} cm^{-3} to 10^{17} cm^{-3}. Specifically, efficiency drops from 22 % at a defect density of 10^{10} cm^{-3} to 0.04 % at 10^{17} cm^{-3} (Fig. 5(a)) and in Fig. 5(b) efficiency declines from 35 % at a defect density of 10^{10} cm^{-3} to 0.01 %

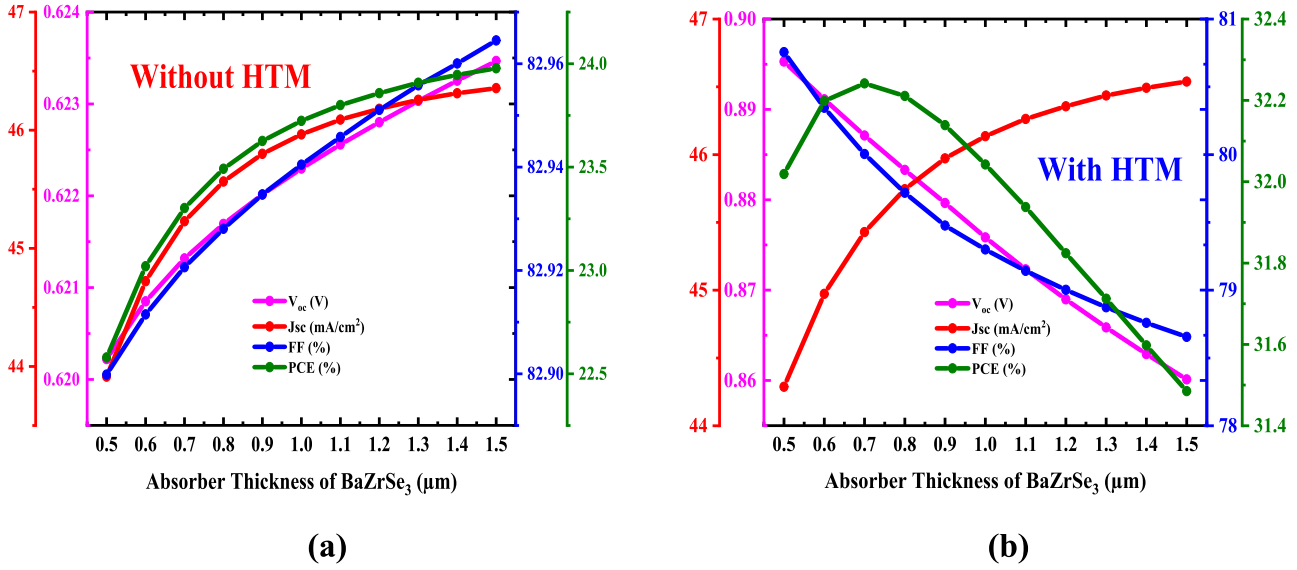

Fig. 3. Results of changing absorber layer thickness on PSCs output (a) without HTM and (b) with SnSe HTM layer.

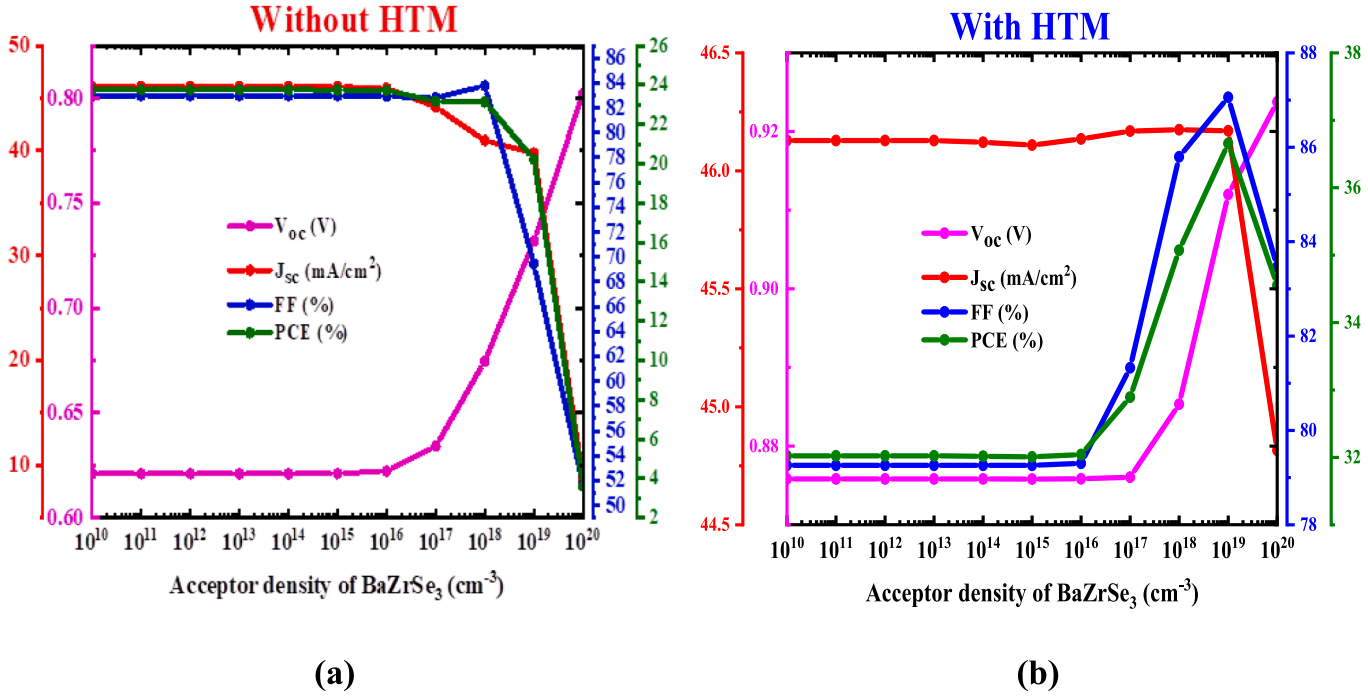

Fig. 4. Effect of varying acceptor concentration of the absorber layer (a) without HTM and (b) with SnSe HTM layer.

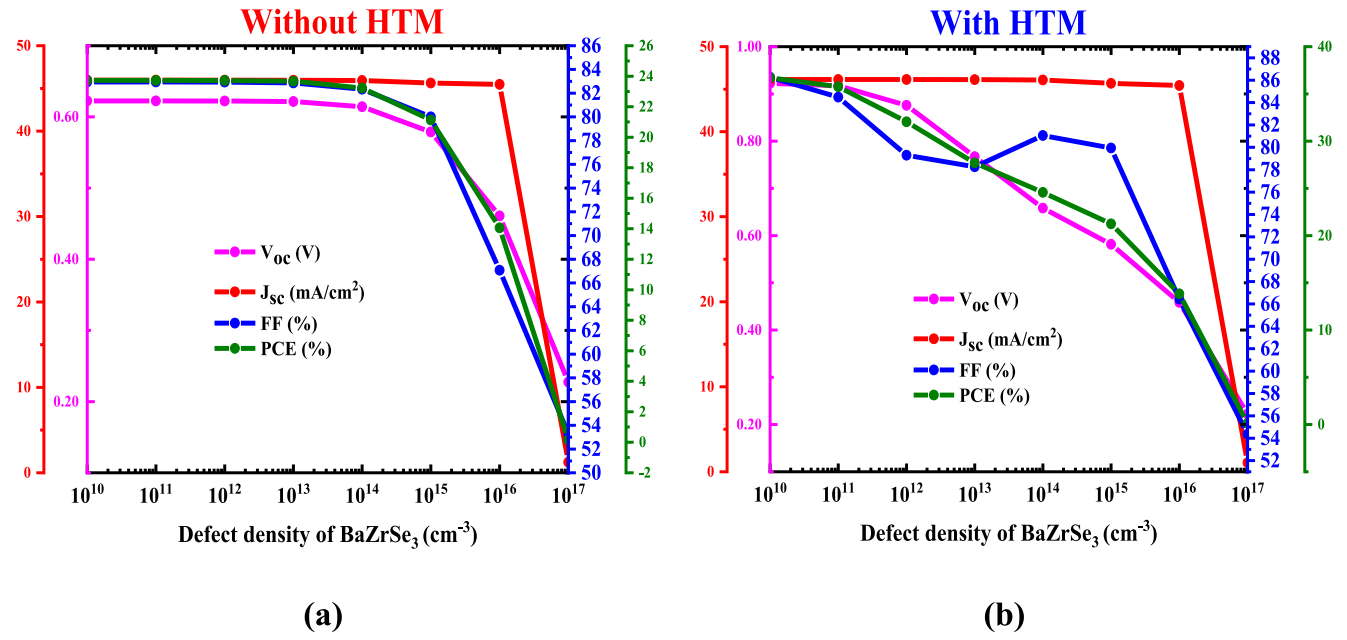

Fig. 5. Result of varying defect density of the absorber layer (a) without HTM and (b) with SnSe HTM layer.

at 10^{17} cm^{-3}. An enhancement of defect density (N_t) diminishes the diffusion length and the carrier lifetime [52,53,54], leading to higher recombination rates in the absorber[55]. Another reason is that the defect function as localized energy levels and act as centers for recombination [56]. Thus, $BaZrSe_3$-based PSCs perform optimally as long as the absorber bulk defect density is below 10^{12} cm^{-3}.

3.5. *Influence of changing thickness of ETM*

This section examines thickness effect of the CdS ETM material on solar cell output as it greatly influences the other electrical properties of the PSCs. Fig. 6(a-b) shows the influences of thickness varied within the range of 0.02 μm to 0.3 μm of ETM layer on the PV parameters of the PSC using previously optimized parameters.

It is explored that as the ETL thickness enhances, J_{sc} diminishes (as depicted in Fig. 6(a)) due to a lessening in the number of photons arriving the absorber, resulting in decreased photocurrent. However, an increased thickness of the ETM layer expands the space charge region, leading to heightened electric field intensity at the ETM/absorber interface and thereby enhancing carrier isolation at this junction [52,53,54]. As a result, there is a rise in V_{oc} (attributed to decreased surface recombination), *FF*, and efficiency (as shown in Fig. 6(a)). Conversely, with the HTM, as the ETM thickness increases, a decrease in both the J_{sc} and the V_{oc} is observed in Fig. 6(b). These are owing to the enhancement of scattering and recombination losses as the distance that the electrons must travel increases. With longer transport distances, the likelihood of electron recombination within the ETM increases, which also contributes to the reduction in *PCE*.

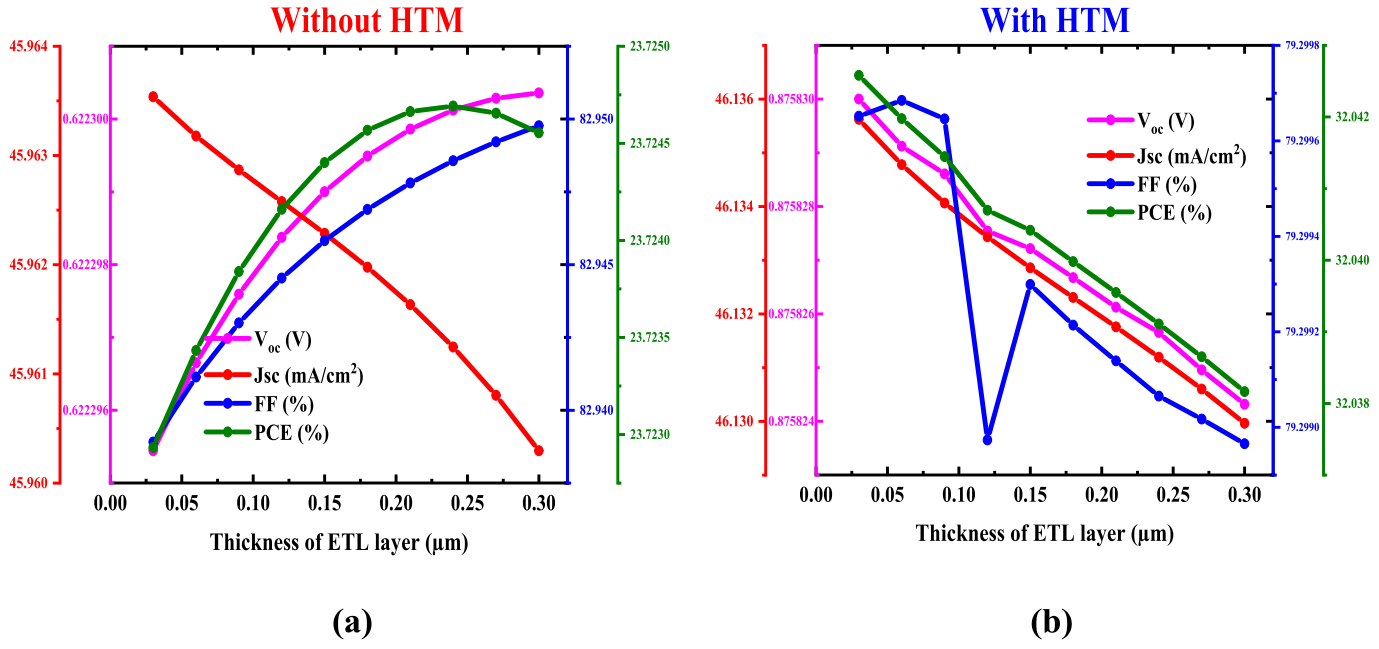

Fig. 6. Impact of changing thickness of the ETM layer (a) without HTM and (b) with SnSe HTM layer.

3.6. Impact of interface defect density on solar cell output

The analysis presented in Sections 3.1 to 3.5 assumed ideal heterojunction interfaces, disregarding the impact of defect density and associated interfacial recombination effects. However, it is essential to evaluate how interfacial (IF) defect density is affected by perovskite solar cell (PSC) performance. Understanding the relationship between IF defect density and key photovoltaic parameters have guided researchers to develop strategies aimed at minimizing defect formation, ultimately improving solar cell efficiency. Additionally, studying the effects of interfacial defects provides deeper insights into the underlying physics of PSCs, opening up pathways for discovering new materials and optimizing fabrication techniques. To further assess the role of IF defects, supplementary simulations were carried out to evaluate the impact of defects at the SnSe/BaZrSe3 and BaZrSe3/CdS interfaces on PSC performance. In these simulations, the IF defect density was varied from 10^{1o} cm^{-2} to 10^{18} cm^{-2}, and the corresponding effects on photovoltaic outputs were analyzed. As shown in Fig. 7(a), increasing the defect density at the SnSe/BaZrSe3 interface led to a substantial reduction in open-circuit voltage (Voc), which dropped from 0.88 V to 0.55 V, and the PCE declined sharply from 32.20 % to 19 %. This decline is attributed to the creation of recombination centers by the IF defects, which disrupt carrier transport and significantly lower both Voc and the fill factor (FF).

Similarly, at the BaZrSe3/CdS interface, the increase in IF defect density had a marked negative impact, as shown in Fig. 7(b). The PCE decreased from 32.20 % to 22.2 %, with a corresponding Voc drop from 0.88 V to 0.62 V, and a slight decrease in short-circuit current density (Jsc) from 46.12 mA/cm^2 to 45.12 mA/cm^2. The primary cause of these performance reductions is trap-assisted recombination at the interface, which limits efficient carrier extraction and transport [57]. These findings underscore the significance of minimizing interfacial defect density to improve PSC performance. The simulation results suggest that an optimal IF defect density of 1 × 101° cm⁻2 is ideal for achieving maximum efficiency, which was applied in this study's simulations to model optimized conditions. These insights help to guide future efforts in improving PSC design and manufacturing, emphasizing the critical role of minimizing defects at material interfaces.

3.7. Effect of series and shunt resistance on the performance of PSCs

The Fig. 8(a-d) depict the impact of series resistance (R_s) and shunt resistance (R_{sh}) on the performance parameters of $BaZrSe_3$-based solar cells, both without an HTM (Fig. 8 (a) and 8 (c)) and with SnSe HTM (Fig. 8 (b) and 8 (d)). In Fig. 8 (a), for the configuration without HTM, the Voc is approximately 0.62 V, and the Jsc is around 45.96 mA/cm^2. As R_s increases to 11 Ω.cm^2, the PCE drops from about 23.63 % to around 8 %, and the fill factor (FF) declines from 82.94 % to 30 % due to higher resistive losses and reduced carrier extraction. Fig. 8 (b), which represents the solar cell with HTM, shows that the Voc remains almost stable at 0.876 V and Jsc at 46.13 mA/cm^2, while PCE and FF decrease as resistance increases, highlighting reduced charge transport. In Fig. 8 (c) and (d), as R_{sh} increases, the cells initially show rapid improvements in PCE and FF due to minimized leakage current and enhanced junction current [58], stabilizing at values around 23.63 % and 32.2 % PCE, and 82.94 % and 79.3 % FF, respectively, for cells without and with HTM. The use of SnSe HTMs enables better carrier collection and reduced recombination losses, as observed by higher Voc and Jsc in the presence of HTMs compared to the non-HTM configuration.

3.8. Influence of temperature on the optimized device performance

Fig. 9 (a-b) illustrates how temperature fluctuations impact the performance of two solar cell devices-one with a hole transport material (HTM) and one without-under solar illumination of 1000 W/m^2, across a temperature range from 250 K to 450 K. As indicated in Fig. 9, key performance metrics such as open-circuit voltage (Voc), fill factor (FF), and power conversion efficiency (PCE) are most affected by increasing temperatures in conventional solar cells [19]. Specifically, Voc decreases as temperature rises due to the increasing reverse saturation current at higher temperatures. Additionally, the elevated temperature leads to the thermal excitation of electrons, which causes atomic vibrations and instability, further promoting carrier recombination and diminishing the cell's efficiency [59]. At a baseline temperature of 300 K, Fig. 9 (a) shows that the solar cell without HTM achieves a Voc of 0.62 V, a PCE of 23.63 %, a short-circuit current density (Jsc) of 45.96 mA/cm^2, and an FF of 82.94 %. In contrast, the optimized device with HTM, as illustrated in Fig. 9 (b), performs significantly better, with a Voc of 0.88 V, a PCE of 32.20 %, a Jsc of 46.14 mA/cm^2, and an FF of 79.30 % at the same temperature of 300 K.

The efficiency of both devices exhibits clear temperature dependence, with PCE declining as the temperature increases. For the optimized PSC with HTM, there is an average reduction in efficiency of approximately −0.05 % per Kelvin (K), which is consistent with findings from previous studies[60]. The primary cause of this efficiency decline is linked to the temperature-induced carrier recombination and reduced

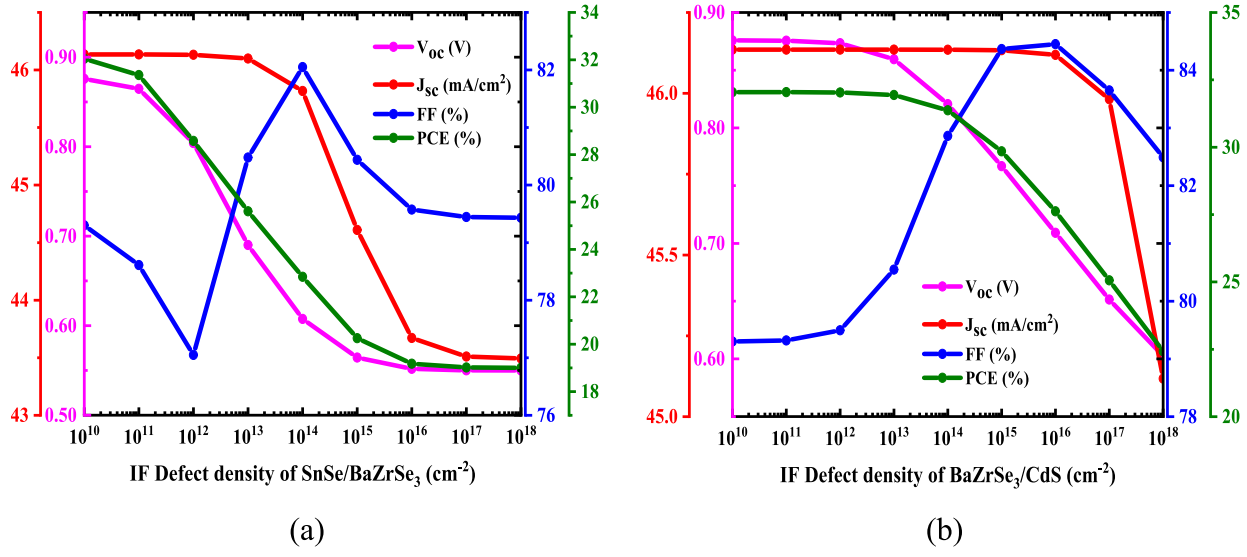

Fig. 7. Impact of interface defect density, (a) SnSe/$BaZrSe_3$ and (b) $BaZrSe_3$/CdS interface on photovoltaic performance parameters.

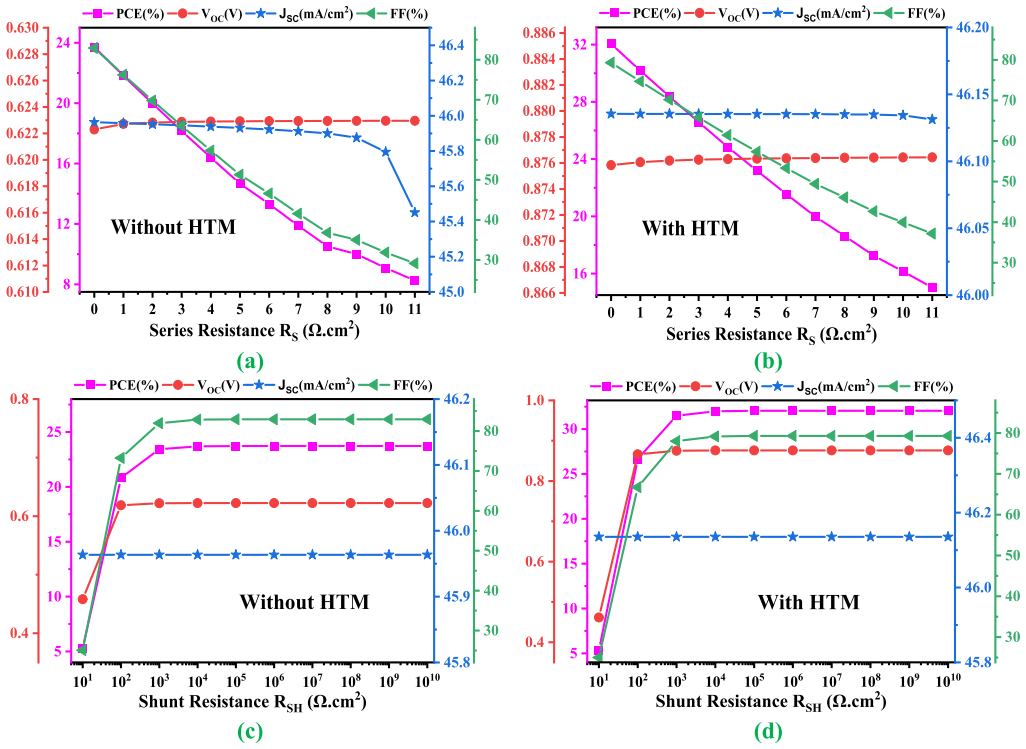

Fig. 8. Effect of series resistance (a) without HTM, (b) with HTM, and shunt resistance (c) without HTM, (d) with HTM on the device performance.

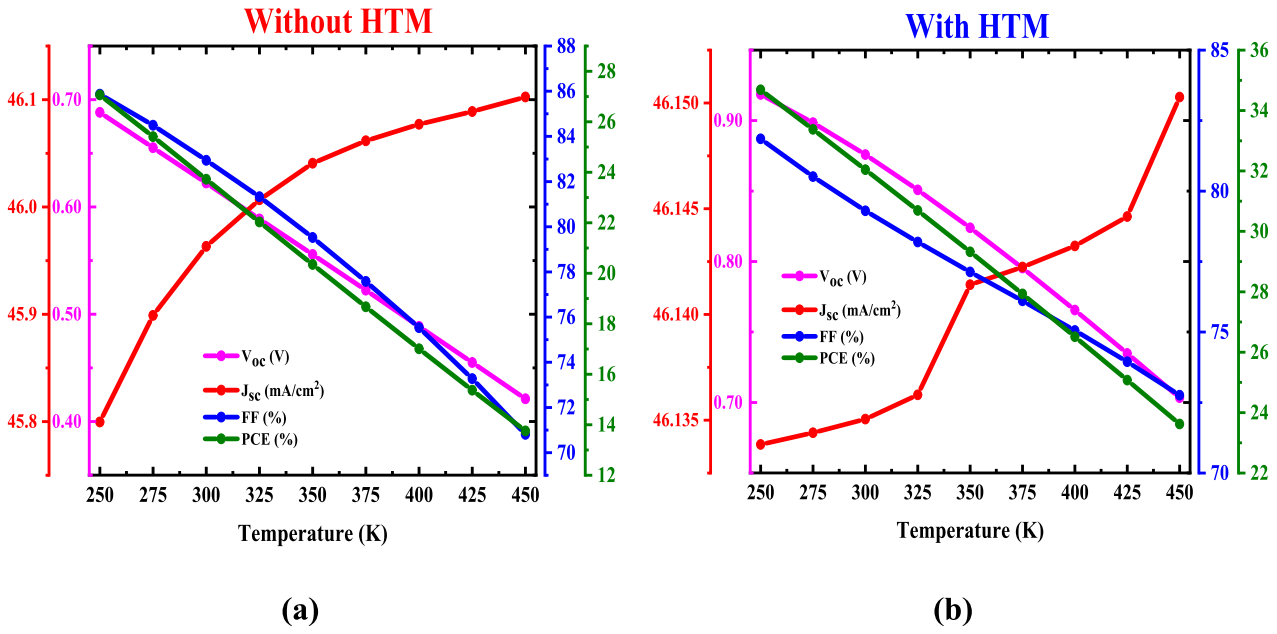

Fig. 9. Influence of temperature on the device (a) without HTM, and (b) the Optimized Device with HTM.

Voc, which together contribute to the degradation of the overall solar cell performance. These results emphasize the importance of temperature management in maintaining high efficiency in solar cells, particularly for devices optimized with HTMs. The use of HTMs, while improving initial performance metrics, does not fully eliminate the adverse effects of temperature variations, highlighting the need for further research into thermal stability and materials that can better resist temperature-related efficiency losses.

3.9. The impact on quantum efficiency (QE) and the J-V characteristics of both PSCs

The inclusion of SnSe as the hole transport material (HTM) in the BaZrSe3-based perovskite solar cell (PSC) structure is crucial for understanding its performance. Fig. 10 (a-b) illustrates the current–voltage (J-V) and quantum efficiency (*QE*) characteristics of BaZrSe3-based solar cells, comparing results for devices both with and without the SnSe HTM. As highlighted in Table 3, there is a significant improvement in both power conversion efficiency (PCE) and fill factor (FF) when SnSe

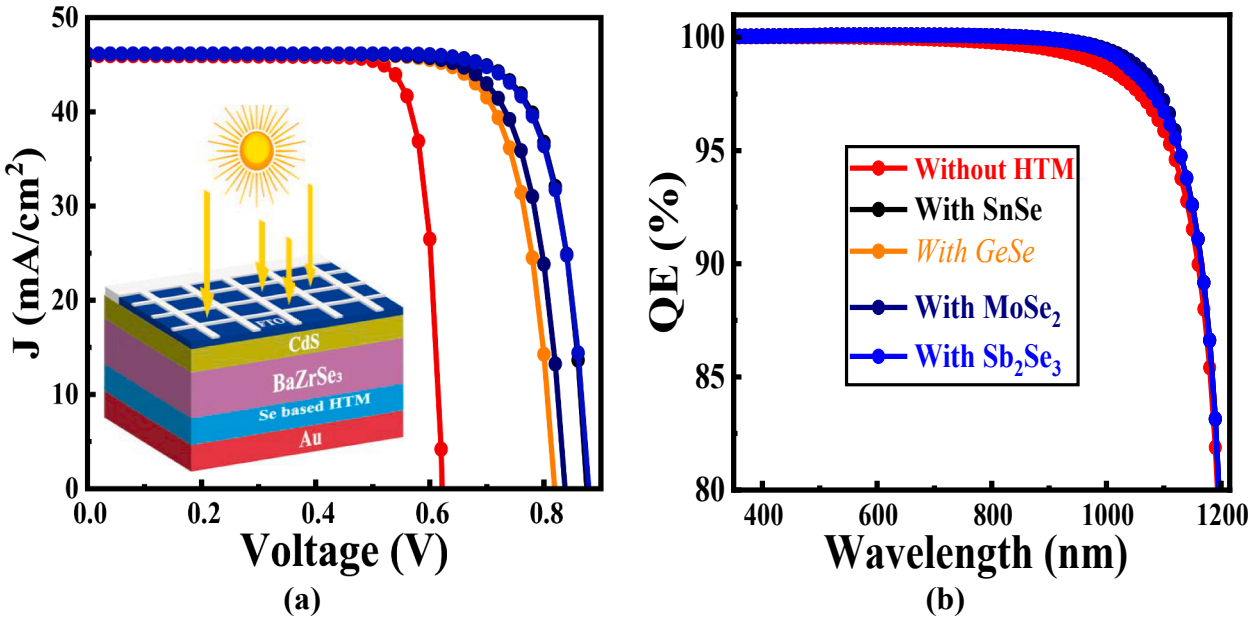

Fig. 10. The comparative analysis includes (a) the J-V curve and (b) the QE for the designed PSC with and without the SnSe HTM.

is used as the HTM. Under optimal conditions, the PCE increases to 32.20 % with the HTM, compared to 23.63 % without it. The presence of the SnSe HTM boosts the overall current output, and the higher open-circuit voltage (Voc) suggests improved electronic properties. This improvement is attributed to a reduction in interfacial recombination of charge carriers between BaZrSe3 and the rear contact metal (gold), along with the excellent charge transport properties of SnSe.

Fig. 10 (b) illustrates the improved *QE* in the device with the SnSe HTM suggests better light absorption and charge carrier extraction efficiency [61,62]. The increased QE in the near-infrared region for the device with HTM indicates improved capability in converting low-energy photons, which boosts the overall performance of the perovskite solar cells (PSCs). Similar high QE trends are observed in other PSC studies [6364–66]. The QE curve shows a sharp drop beyond 1200 nm, aligning with the 1.01 eV band gap of $BaZrSe_3$. Variations in QE response are likely due to the formation of a back surface field after integrating the HTM. $BaZrSe_3$ serves as both the absorber and the p-type semiconductor layer, while adding another p-type layer (SnSe) enhances the PSC's output parameters, highlighting SnSe's importance as an HTM for optimal PSC performance.

4. Conclusions

The FTO/CdS/$BaZrSe_3$/SnSe/Au structure was simulated using SCAPS-1D software to optimize the performance of the perovskite solar cell (PSC). The simulations revealed that efficiency could be significantly improved by fine-tuning the thickness and carrier concentration of the absorber material and the thickness of the hole transport material (HTM). The ideal thicknesses were determined to be 1 μm for the absorber layer and 0.1 μm for the HTM, with an optimized doping density of 1.0×10^{16} cm^{-3} for both layers. Among the HTMs tested, SnSe showed the best band alignment and carrier transport properties, leading to power conversion efficiency (PCE) of approximately 32.20 % in the optimized device. This was achieved with a short-circuit current density (Jsc) of around 46.14 mA/cm^2, an open-circuit voltage (Voc) of 0.88 V, and a fill factor (FF) of 79.30 %. The optimized doping density of 1×10^{16} cm^{-3} is consistent with the ideal doping level for $BaZrSe_3$. The built-in potential of the $BaZrSe_3$-based PSC was also found to be 0.88 V. In comparison, $BaZrSe_3$-based PSCs without the SnSe HTM (FTO/CdS/$BaZrSe_3$/Au) achieved a lower PCE of 23.63 %. These results highlight the potential of $BaZrSe_3$-based PSCs as a promising alternative to traditional lead-based perovskites, offering a pathway to more sustainable and high-performance solar energy solutions.

5. Data availability statement

The data that support the findings of this study are available from the corresponding author upon reasonable request.

CRediT authorship contribution statement

Md Masum Mia: Writing – review & editing, Writing – original draft, Visualization, Software, Resources, Formal analysis, Data curation. **Md. Faruk Hossain:** Writing – review & editing, Writing – original draft, Visualization, Validation. **Mahabur Rahman:** Writing – review & editing, Writing – original draft, Visualization, Validation, Software, Resources, Data curation. **Nacer Badi:** Writing – review & editing, Writing – original draft, Visualization, Validation. **Ahmad Irfan:** Writing – review & editing, Writing – original draft, Visualization, Validation. **Md. Ferdous Rahman:** Writing – review & editing, Writing – original draft, Visualization, Validation, Supervision, Software, Resources, Methodology, Formal analysis, Data curation, Conceptualization.

Declaration of competing interest

The authors declare that they have no known competing financial interests or personal relationships that could have appeared to influence the work reported in this paper.

Acknowledgments

A. Irfan extends his appreciation to the Deanship of Research and Graduate Studies at King Khalid University for funding this work through Large Research Project under grant number RGP2/146/45.

Data availability

Data will be made available on request.

References

[1] N. Kannan, D. Vakeesan, Solar energy for future world: - A review, Renew. Sustain. Energy Rev. 62 (2016) 1092–1105, https://doi.org/10.1016/j.rser.2016.05.022.

[2] A. Ait Abdelkadir, M. Sahal, Theoretical development of the CZTS thin-film solar cell by SCAPS-1D software based on experimental work, Mater. Sci. Eng. B 296 (2023) 116710, https://doi.org/10.1016/j.mseb.2023.116710.

[3] J. Liang, Y. Wang, Y. Zhang, X. Liu, J. Lin, Construction of perovskite homojunction for highly efficient perovskite solar cells by SCAPS-1D, Mater. Sci. Eng. B 301 (2024) 117196, https://doi.org/10.1016/j.mseb.2024.117196.

[4] B. Sultana, F. Rahman, A. Chandra, M. Mia, A. Ijajul, A. Irfan, A. Rasool, D. Haque, Materials Science & Engineering B A novel design and optimization of Si based high performance double absorber heterojunction solar cell, Mater. Sci. Eng. B 304 (2024) 117360, https://doi.org/10.1016/j.mseb.2024.117360.

[5] C.O. Teixeira, D. Castro, L. Andrade, A. Mendes, Selection of the ultimate perovskite solar cell materials and fabrication processes towards its industrialization: A review, Energy Sci. Eng. 10 (2022) 1478–1525, https://doi.org/10.1002/ese3.1084.

[6] Adv Funct Materials - 2023 - Yan - A Polymer-in-Salt Solid Electrolyte Enabled by Fast Phase Transition Route for .pdf, (n.d.).

[7] L. Song, Y. Fan, H. Fan, X. Yang, K. Yan, X. Wang, L. Ma, Photo-assisted rechargeable metal batteries, Nano Energy 125 (2024) 109538, https://doi.org/10.1016/j.nanoen.2024.109538.

[8] L. Lv, L. Lei, Q.W. Chen, C.L. Yin, H. Fan, J.P. Zhou, Oxygen vacancies-modified S-scheme heterojunction of Bi-doped La2Ti2O7 and La-doped Bi4Ti3O12 to improve the NO gas removal avoiding NO2 product, Appl. Catal. B Environ. 343 (2024) 3, https://doi.org/10.1016/j.apcatb.2023.123464.

[9] S. Cui, X. Ren, H. Yin, H. Fan, C. Wang, M. Zhang, Y. Tang, H. Yuan, Y. Xin, One-step electrodeposited nickel-cobalt-layered double hydroxide nanosheets with anion intercalation for supercapacitor, J. Energy Storage 85 (2024) 111092, https://doi.org/10.1016/j.est.2024.111092.

[10] [10] M.F. Rahman, M.K. Hasan, M. Chowdhury, M.R. Islam, M.H. Rahman, M.A. Rahman, S.R. Al Ahmed, A.B.M. Ismail, M. Amami, M.K. Hossain, G.A.A.M. Al-Hazmi, A qualitative Design and optimization of CIGS-based Solar Cells with Sn2S3 Back Surface Field: A plan for achieving 21.83 % efficiency, Heliyon 9 (2023) e22866. DOI: 10.1016/J.HELIYON.2023.E22866.

[11] M.F. Rahman, M. Chowdhury, L. Marasamy, M.K.A. Mohammed, M.D. Haque, S. R. Al Ahmed, A. Irfan, A.R. Chaudhry, S. Goumri-Said, Improving the efficiency of a CIGS solar cell to above 31% with Sb2S3 as a new BSF: a numerical simulation approach by SCAPS-1D, RSC Adv. 14 (2024) 1924–1938, https://doi.org/10.1039/d3ra07893k.

[12] M. Rahman, M. Habib, M. Ali, M. Rubel, M.R. Islam, A.B.M. Ismail, M.K. Hossain, Design and numerical investigation of cadmium telluride (CdTe) and iron silicide (FeSi2) based double absorber solar cells to enhance power conversion efficiency, AIP Adv. 12 (2022), https://doi.org/10.1063/5.0108459.

[13] A.D. Adewoyin, M.A. Olopade, M. Chendo, Enhancement of the conversion efficiency of Cu2ZnSnS4 thin film solar cell through the optimization of some device parameters, Optik (stuttg). 133 (2017) 122–131, https://doi.org/10.1016/j.ijleo.2017.01.008.

[14] M. Ferdous Rahman, M. Naim Hasan Toki, A. Kuddus, M.K.A. Mohammed, M. Rasidul Islam, S. Bhattarai, J. Madan, R. Pandey, R. Marzouki, M. Jemmali, Boosting efficiency above 30 % of novel inorganic Ba3SbI3 perovskite solar cells with potential ZnS electron transport layer (ETL), Mater. Sci. Eng. B 300 (2024) 117073, https://doi.org/10.1016/j.mseb.2023.117073.

[15] M. Luo, J. Luo, J. Dong, A. Yang, Z. Xie, Structural, electronic, optical, and mechanical properties of the all-inorganic lead-free metal halides double perovskites Cs2RbInX6 (X = Cl, Br, I): A first-principles based study, Mater. Sci. Eng. B 290 (2023) 116299, https://doi.org/10.1016/j.mseb.2023.116299.

[16] E. Ojeda-Durán, K. Monfil-Leyva, J. Andrade-Arvizu, I. Becerril-Romero, Y. Sánchez, R. Fonoll-Rubio, M. Guc, Z. Jehl, J.A. Luna-López, A.L. Muñoz-Zurita, J.A.D. Hernández-de la Luz, V. Izquierdo-Roca, M. Placidi, E. Saucedo, CZTS solar cells and the possibility of increasing VOC using evaporated Al2O3 at the CZTS/CdS interface, Sol. Energy 198 (2020) 696–703, https://doi.org/10.1016/j.solener.2020.02.009.

[17] M. Noman, M. Shahzaib, S.T. Jan, Z. Khan, M. Ismail, A.D. Khan, Optimizing band gap, electron affinity, & carrier mobility for improved performance of formamidinium lead tri-iodide perovskite solar cells, Mater. Sci. Eng. B 300 (2024) 117114, https://doi.org/10.1016/j.mseb.2023.117114.

[18] R. Rani, K. Monga, S. Chaudhary, Recent development in electron transport layers for efficient tin-based perovskite solar cells, IOP Conf. Ser. Mater. Sci. Eng. 1258 (2022) 012015, https://doi.org/10.1088/1757-899x/1258/1/012015.

[19] M.F. Rahman, A. Lubaba, L. Ben Farhat, S. Ezzine, M.H. Rahman, M. Harun-Or-Rashid, Efficiency enhancement above 31 % of Sb2Se3 solar cells with optimizing various BSF layer, Mater. Sci. Eng. B 307 (2024) 117527, https://doi.org/10.1016/j.mseb.2024.117527.

[20] N. Thakur, P. Kumar, P. Sharma, Simulation study of chalcogenide perovskite (BaZrSe3) solar cell by SCAPS-1D, Mater. Today Proc. (2023), https://doi.org/10.1016/j.matpr.2023.01.012.

[21] Y. Wang, N. Sato, K. Yamada, T. Fujino, Synthesis of BaZrS3 in the presence of excess sulfur, J. Alloys Compd. 311 (2000) 214–223, https://doi.org/10.1016/S0925-8388(00)01134-8.

[22] Y.-Y. Sun, M.L. Agiorgousis, P. Zhang, S. Zhang, Chalcogenide perovskites for photovoltaics, Nano Lett. 15 (2015) 581–585.

[23] T. Gupta, D. Ghoshal, A. Yoshimura, S. Basu, P.K. Chow, A.S. Lakhnot, J. Pandey, J. M. Warrender, H. Efstathiadis, A. Soni, An Environmentally Stable and Lead-Free Chalcogenide Perovskite, Adv. Funct. Mater. 30 (2020) 2001387.

[24] M. Ong, D.M. Guzman, Q. Campbell, I. Dabo, R.A. Jishi, BaZrSe 3: Ab initio study of anion substitution for bandgap tuning in a chalcogenide material, J. Appl. Phys. 125 (2019), https://doi.org/10.1063/1.5097940.

[25] S.B. Sabine Körbel, M.A.L. Marques, Stability and electronic properties of new inorganic perovskites from high-throughput ab initio calculations, J. Mater. Chem. C 4 (2016) 3157–3167, https://doi.org/10.1039/C5TC04172D.

[26] A. Aissat, L. Chenini, A. Laidouci, S. Nacer, J.P. Vilcot, Improvement in the efficiency of solar cells based on the ZnSnN2/Si structure, Mater. Sci. Eng. B 300 (2024) 117071, https://doi.org/10.1016/j.mseb.2023.117071.

[27] M. Ferdous Rahman, M. Al Ijajul Islam, M. Chowdhury, L. Ben Farhat, S. Ezzine, A. T.M. Saiful Islam, Efficiency improvement of CsSnI3 based heterojunction solar cells with P3HT HTL: A numerical simulation approach, Mater. Sci. Eng. B 307 (2024) 117524, https://doi.org/10.1016/j.mseb.2024.117524.

[28] K. Yumigeta, C. Brayfield, H. Cai, D. Hajra, M. Blei, S. Yang, Y. Shen, S. Tongay, The synthesis of competing phase GeSe and GeSe $_2$ 2D layered materials, RSC Adv. 10 (2020) 38227–38232, https://doi.org/10.1039/D0RA07539F.

[29] F. Arif, M. Aamir, A. Shuja, M. Shahiduzzaman, J. Akhtar, Simulation and numerical modeling of high performance CH3NH3SnI3 solar cell with cadmium sulfide as electron transport layer by SCAPS-1D, Results Opt. 14 (2024) 100595, https://doi.org/10.1016/j.rio.2023.100595.

[30] M. Burgelman, P. Nollet, S. Degrave, Modelling polycrystalline semiconductor solar cells, Thin Solid Films 361–362 (2000) 527–532, https://doi.org/10.1016/S0040-6090(99)00825-1.

[31] Y. Wei, Z. Ma, X. Zhao, J. Yin, Y. Wu, L. Zhang, M. Zhao, Improving the performance of Cu2ZnSn(S, Se)4 thin film solar cells by SCAPS simulation, Mater. Sci. Eng. B 303 (2024) 117296, https://doi.org/10.1016/j.mseb.2024.117296.

[32] A. Samavati, A. Awang, Z. Samavati, A. Fauzi Ismail, M.H.D. Othman, M. Velashjerdi, G.B. Eisaabadi, A. Rostami, Influence of ZnO nanostructure configuration on tailoring the optical bandgap: Theory and experiment, Mater. Sci. Eng. B 263 (2021) 114811, https://doi.org/10.1016/j.mseb.2020.114811.

[33] M.F. Rahman, M.A. Monnaf, M. Amami, L. Ben Farhat, M.A. Rahman, Improving the efficiency above 35% of MoS2-based solar cells by through optimization of various wide-bandgap S-chalcogenides ETL, J. Phys. Chem. Solids (2024) 112216, https://doi.org/10.1016/j.jpcs.2024.112216.

[34] N. Nahid, S. Shah, H. Mamur, R. Hosen, Chemistry of Inorganic Materials Optimizing lead-free CH 3 NH 3 SnI 3 perovskite solar cells by using SCAPS-1D software, Chem. Inorg. Mater. 4 (2024) 100069, https://doi.org/10.1016/j.cinorg.2024.100069.

[35] A. Bala Sairam, Y. Singh, M. Mamta, S. Kumar, V.N.S. Rani, Investigation of Different Configurations in GeSe Solar Cells for Their Performance Improvement, J. Nanomater. (2023 (2023).), https://doi.org/10.1155/2023/9266072.

[36] A. Ghobadi, M. Yousefi, M. Minbashi, A.H.A. Kordbacheh, A.H. Abdolvahab, N. E. Gorji, Simulating the effect of adding BSF layers on Cu2BaSnSSe3 thin film solar cells, Opt. Mater. (amst). 107 (2020), https://doi.org/10.1016/j.optmat.2020.109927.

[37] T. Ahmed, M.C. Islam, M.A.H. Pappu, S.K. Mostaque, B.K. Mondal, J. Hossain, A highly efficient <scp>n-CdS</scp> / <scp> p-Ag 2 S </scp> /p + - <scp>SnS</scp> thin film solar cell: Design and simulation, Eng. Reports (2024), https://doi.org/10.1002/eng2.12849.

[38] N. Thakur, P. Kumar, R. Neffati, P. Sharma, Design and simulation of chalcogenide perovskite BaZr(S, Se) 3 compositions for photovoltaic applications, Phys. Scr. 98 (2023) 065921, https://doi.org/10.1088/1402-4896/accfc6.

[39] M.F. Rahman, M.M. Alam Moon, M.K. Hossain, M.H. Ali, M.D. Haque, A. Kuddus, J. Hossain, A.B. Abu, Concurrent investigation of antimony chalcogenide (Sb2Se3 and Sb2S3)-based solar cells with a potential WS2 electron transport layer, Heliyon 8 (2022) e12034. DOI: 10.1016/j.heliyon.2022.e12034.

[40] V. Deswal, S. Kaushik, R. Kundara, S. Baghel, Numerical simulation of highly efficient Cs2AgInBr 6-based double perovskite solar cell using SCAPS 1-D, Mater. Sci. Eng. B 299 (2024) 117041, https://doi.org/10.1016/j.mseb.2023.117041.

[41] M. Hassan, S.A. Rouf, A.S. Alofi, Q. Mahmood, A. Ishfaq, M. mana AL-Anazy, A. S. Alshomrany, M. Ferdous Rahman, E. Sayed Yousef, Impact of terbium (Tb) on ferromagnetism and thermoelectric behaviour of spinels MgTb2(S/Se)4 for spintronic, Mater. Sci. Eng. B 300 (2024) 117110, https://doi.org/10.1016/j.mseb.2023.117110.

[42] N. Marinova, W. Tress, R. Humphry-Baker, M.I. Dar, V. Bojinov, S.M. Zakeeruddin, M.K. Nazeeruddin, M. Grätzel, Light Harvesting and Charge Recombination in CH $_3$ NH $_3$ PbI $_3$ Perovskite Solar Cells Studied by Hole Transport Layer Thickness Variation, ACS Nano 9 (2015) 4200–4209, https://doi.org/10.1021/acsnano.5b00447.

[43] I. Chabri, A. Oubelkacem, Y. Benhouria, A. Kaiba, I. Essaoudi, A. Ainane, Performance optimization of a CsGeI3-based solar device by numerical simulation, Mater. Sci. Eng. B 297 (2023) 116757, https://doi.org/10.1016/j.mseb.2023.116757.

[44] M.M. Ivashchenko, O.V. Diachenko, A.S. Opanasyuk, I.P. Buryk, D.V. Kuzmin, A. Čerškus, O. Shapovalov, S.V. Plotnikov, I.A. Gryshko, A numerical simulation of solar cells based on the CuO and Cu2O absorber layers with ZnMgO window layer, Mater. Sci. Eng. B 300 (2024) 117133, https://doi.org/10.1016/j.mseb.2023.117133.

[45] G.A. Casas, M.A. Cappelletti, A.P. Cédola, B.M. Soucase, E.L., Peltzer y Blancá, Analysis of the power conversion efficiency of perovskite solar cells with different materials as Hole-Transport Layer by numerical simulations, Superlattices Microstruct. 107 (2017) 136–143, https://doi.org/10.1016/j.spmi.2017.04.007.

[46] B. Sun, L. Zhang, T. Zhou, C. Shao, L. Zhang, Y. Ma, Q. Yao, Z. Jiang, F.A. Selim, H. Chen, Protected-annealing regulated defects to improve optical properties and luminescence performance of Ce:YAG transparent ceramics for white LEDs, J. Mater. Chem. C 7 (2019) 4057–4065, https://doi.org/10.1039/C8TC06600K.

[47] R. Indirajith, M. Rajalakshmi, R. Gopalakrishnan, K. Ramamurthi, Effects of annealing on thermally evaporated SnSe thin films, Ferroelectrics 413 (2011) 108–114, https://doi.org/10.1080/00150193.2011.551090.
[48] N. Shahzad, N. Ali, I. Haq, S.W. Shah, S. Ali, Q.S. Ahmad, F. Azlullah, A. Kalam, A. G. Al-Sehemi, ANNEALED TIN SELENIDE (SnSe) THIN FILM MATERIAL FOR SOLAR CELL APPLICATION, 2020.
[49] M.S. Islam, M.F. Rahman, M.R. Islam, A. Ghosh, M.A. Monnaf, M.S. Reza, M. K. Hossain, A. Zaman, S. Ezzine, L. Ben Farhat, An in-depth analysis of how strain impacts the electronic, optical, and output performance of the Ca3NI3 novel inorganic halide perovskite, J. Phys. Chem. Solids 185 (2024) 111791, https://doi.org/10.1016/j.jpcs.2023.111791.
[50] Z. Omarova, D. Yerezhep, A. Aldiyarov, N. Tokmoldin, In Silico Investigation of the Impact of Hole-Transport Layers on the Performance of CH3NH3SnI3 Perovskite Photovoltaic Cells, Crystals 12 (2022), https://doi.org/10.3390/cryst12050699.
[51] E.K. Katunge, G.G. Njema, J.K. Kibet, Theoretical analysis of the electrical characteristics of lead-free formamidinium tin iodide solar cell, IET Optoelectron. 17 (2023) 220–236, https://doi.org/10.1049/ote2.12104.
[52] M. Courel, M.M. Nicolás-Marín, Analysis of The Eciency In Sb2Se3 Thin-Film Solar Cells Using Alternative Buffer Layers In n-p and n-i-p Structures By Numerical Simulation. F Ayala-Mato (fayala840425@gcom) Universidad Autónoma del Estado de Morelos https://orcid.org/0000-0003-4, (n.d.). DOI: 10.21203/rs.3.rs-644062/v1.
[53] P.G.D.K. Ngue, A.T. Ngoupo, A.M.N. Abena, F.X.A. Abega, J.-M.-B. Ndjaka, Investigation of the Performance of a Sb2S3-Based Solar Cell with a Hybrid Electron Transport Layer (h-ETL): A Simulation Approach Using SCAPS-1D Software, Int. J. Photoenergy 2024 (2024) 1–23, https://doi.org/10.1155/2024/5188636.
[54] S. Abdelaziz, A. Zekry, A. Shaker, M. Abouelatta, Investigation of lead-free MASnI3-MASnIBr 2 tandem solar cell: Numerical simulation, Opt. Mater. (amst). 123 (2022) 111893, https://doi.org/10.1016/j.optmat.2021.111893.
[55] T. Ouslimane, L. Et-taya, L. Elmaimouni, A. Benami, Impact of absorber layer thickness, defect density, and operating temperature on the performance of MAPbI3 solar cells based on ZnO electron transporting material, Heliyon 7 (2021) e06379. DOI: 10.1016/j.heliyon.2021.e06379.
[56] M.M. Khatun, A. Sunny, S.R. Al Ahmed, Numerical investigation on performance improvement of WS2 thin-film solar cell with copper iodide as hole transport layer, Sol. Energy 224 (2021) 956–965, https://doi.org/10.1016/j.solener.2021.06.062.
[57] W. Abdelaziz, A. Shaker, M. Abouelatta, A. Zekry, Possible efficiency boosting of non-fullerene acceptor solar cell using device simulation, Opt. Mater. (amst) 91 (2019) 239–245, https://doi.org/10.1016/j.optmat.2019.03.023.
[58] M.K. Hossain, M.H.K. Rubel, G.F.I. Toki, I. Alam, M.F. Rahman, H. Bencherif, Effect of Various Electron and Hole Transport Layers on the Performance of CsPbI3-Based Perovskite Solar Cells: A Numerical Investigation in DFT, SCAPS-1D, and wxAMPS Frameworks, ACS Omega 7 (2022) 43210–43230, https://doi.org/10.1021/acsomega.2c05912.
[59] Y.H. Khattak, F. Baig, S. Ullah, B. Marí, S. Beg, H. Ullah, Enhancement of the conversion efficiency of thin film kesterite solar cell, J. Renew. Sustain. Energy 10 (2018), https://doi.org/10.1063/1.5023478.
[60] A. Sunny, S. Rahman, M.M. Khatun, S.R. Al Ahmed, Numerical study of high performance HTL-free CH3NH3SnI3-based perovskite solar cell by SCAPS-1D, AIP Adv. 11 (2021), https://doi.org/10.1063/5.0049646.
[61] E. Oublal, A. Ait Abdelkadir, M. Sahal, High performance of a new solar cell based on carbon nanotubes with CBTS compound as BSF using SCAPS-1D software, J. Nanoparticle Res. 24 (2022), https://doi.org/10.1007/s11051-022-05580-7.
[62] N. Rahman, A. Bakkar, M.D. Haque, S.R. Al Ahmed, M.H. Rahman, A. Irfan, A. R. Chaudhry, M.F. Rahman, Impact of CdTe BSF layer on enhancing the efficiency of MoSe2 solar cell, J. Opt. (2024), https://doi.org/10.1007/s12596-024-01855-5.
[63] E. Danladi, P.M. Gyuk, N.N. Tasie, A.C. Egbugha, D. Behera, I. Hossain, I.M. Bagudo, M.L. Madugu, J.T. Ikyumbur, Impact of hole transport material on perovskite solar cells with different metal electrode: A SCAPS-1D simulation insight, Heliyon 9 (2023) e16838. DOI: 10.1016/j.heliyon.2023.e16838.
[64] M.K. Hossain, M.H.K. Rubel, G.F.I. Toki, I. Alam, M.F. Rahman, H. Bencherif, Effect of Various Electron and Hole Transport Layers on the Performance of CsPbI 3 -Based Perovskite Solar Cells: A Numerical Investigation in DFT, SCAPS-1D, and wxAMPS Frameworks, ACS Omega 7 (2022) 43210–43230, https://doi.org/10.1021/acsomega.2c05912.
[65] S. Mushtaq, S. Tahir, A. Ashfaq, R. Sebastian Bonilla, M. Haneef, R. Saeed, W. Ahmad, N. Amin, Performance optimization of lead-free MASnBr 3 based perovskite solar cells by SCAPS-1D device simulation, Sol. Energy 249 (2023) 401–413, https://doi.org/10.1016/j.solener.2022.11.050.
[66] S. Khatoon, V. Chakraborty, S.K. Yadav, S. Diwakar, J. Singh, R.B. Singh, Simulation study of CsPbIxBr 1–x and MAPbI3 heterojunction solar cell using SCAPS-1D, Sol. Energy 254 (2023) 137–157, https://doi.org/10.1016/j.solener.2023.02.059.